Composite Structures 269 (2021) 114004

Contents lists available at ScienceDirect

Composite Structures

journal homepage: www.elsevier.com/locate/compstruct

Macro- and micro-instabilities in incompressible bioinspired composite materials with nacre-like microstructure

Fabrizio Greco [a], Lorenzo Leonetti [a], Umberto De Maio [a], Stephan Rudykh [b,*], Andrea Pranno [a,b]

[a] Department of Civil Engineering, University of Calabria, Rende, Italy
[b] Department of Mechanical Engineering, University of Wisconsin-Madison, Madison, WI, USA

ARTICLE INFO

Keywords:
Bio-inspired composites
Nacre-like microstructure
Finite deformation
Instability
Microscopic instabilities
Loss of ellipticity

ABSTRACT

In this work, we study the macroscopic and microscopic instabilities in 2D incompressible nacre-like composite materials induced by uniaxial loadings. The interchange between macro- and micro-instabilities in bioinspired composite materials has been investigated by examining different combinations of platelets volume fraction, aspect ratio, and shear modulus contrast between the stiff (platelets) and soft (matrix) phases. It has been highlighted that the critical instability mode shapes, together with their critical load factors and wavelengths, are highly influenced by the microscopic geometrical arrangement and the material composition. For a wide range of geometrical and material parameters, the instabilities are found to be global with an in-phase mode shape. It has been shown that the out-of-phase instability mode shapes occur at a significantly higher magnitude of the homogenized energy compared to the in-phase ones. The results indicate that, adopting a small unit cell assembly, the microscopic stability analysis provides in most of cases strong underestimates of the critical stretch ratios, and that an accurate and efficient instability prediction can be instead obtained based on the loss of strong ellipticity condition of the homogenized incremental moduli tensor, except for few cases in which local modes occur.

1. Introduction

Natural materials, such as wood, bones and shells, aided the scientific progress in its early stages, but these materials were steadily replaced by synthetic composite materials reinforced by means of particles, fibers or platelets that have been intensely investigated in the past decade with the aim to satisfy the industrial request to achieve superior mechanical, optical, electrical, magnetic, and thermal properties [1–4]. Engineers and scientists today continue to be attracted by the remarkable characteristics of natural structures which, in the light of their microstructural heterogeneity, can both be lightweight and offer mechanical properties exceeding those of their microstructural parts [5–7]. In parallel to this, the advanced technologies landed in the field of additive manufacturing allowed to produce innovative composite materials characterized by complex microstructures. Therefore, the combination of these events, together with the availability of modern modeling tools, pulled the researchers to investigate the intricate interplay of the mechanisms operating in such natural materials on various observation scales, from the nanoscopic scale to the macroscopic one, promoting thus the development of new research lines based on the mechanical characterization of composite materials whose microstructure is inspired by the nature [8–11]. The nacre microstructure represents one of the most studied microgeometrical arrangements in the light of the excellent combination of high strength and toughness properties achieved at the macroscopic scale and it provided a rich source of inspiration for designing high-performance materials. The excellent properties of nacre-like materials are based on the unique arrangement of stiff aligned mineral platelets (reinforcement) linked together by a soft organic interface (matrix) in a brick and mortar scheme [12,13], leading to a particular class of bioinspired materials whose macroscopic properties are derived from their hierarchical structure. Since nacre-like composite materials are heterogeneous solids belonging to the class of the microstructured composite materials, quite recently considerable attention has been paid to the investigation of the nonlinear phenomena characterizing such material class. Generally speaking, such composite materials, if subjected to extreme loading processes, show microstructural evolutions due to, for instance, the occurrence of nonlinear phenomena such as interface debonding, coalescence of micro-cracks and delamination [14–17], or due to the onset of geometrical or material nonlinearities induced by

* Corresponding author.
E-mail address: rudykh@wisc.edu (S. Rudykh).

https://doi.org/10.1016/j.compstruct.2021.114004
Received 13 January 2021; Accepted 15 April 2021
Available online 19 April 2021

large deformations [18–20]. The material models commonly adopted for 3D printed nacre-like composite materials belong to the class of hyperelastic models. For several years great effort has been devoted to the study of the macroscopic nonlinear behavior of undamaged hyperelastic material models subjected to nonlinear phenomena at the microstructural scale [21–26] and subjected to the combination of different microscopic failure phenomena such as both instability and fracture [27–30]. The study of the macroscopic response of microstructured composite materials considering different kinds of microscopic nonlinear phenomena requires overwhelming computational effort due to the necessity to model all the microstructural details. About that, several publications have appeared in the past years highlighting efficient modeling techniques requiring the development of advanced numerical procedures based on FEM in the framework of small and large deformations to reduce the computational effort needed to model every phenomenon acting at the microstructural scale, for instance, the classical homogenization techniques [31–34] and the multiscale approaches [35–39]. Such advanced computational techniques are not still adopted frequently to investigate the behavior of bioinspired composite material such as nacre-like composites but, recently, in a previous work by some of the authors, a multiscale strategy was proposed to predict the mechanical behavior of the composite material and, in a large deformation context, the best compromise between penetration resistance and flexibility was identified with the aim to design a body protective bio-inspired material architecture [40]. Numerous authors have reported also that the physical behavior of nacre-like materials is mainly characterized by the platelets' interaction and that their superior properties are usually provided by several mechanisms operating on separate length scales [41]. The matrix, identified as the soft phase of the heterogeneous solid, represents the main component that affects the mechanical performance of such a natural composite [42,43] due to the fact that, in every deformation process, it regulates the interaction between the platelets (identified as the stiff phase). Some works have shown that the weakest part of such materials is the interface between the soft and the stiff phases, and thus several models have been developed to investigate the damage mechanisms in nacre-like materials subjected to extreme loading processes [44]. For instance in [45] a discrete element approach using rigid brick elements with cohesive zone interactions has been developed and, more recently, in [46] the effect of the interfaces on both mechanical strength and fracture toughness has been investigated with the aim to provide design guidelines for synthetic nacre-like composite materials. Definitively, the literature on the mechanical characterization of nacre-like composite materials shows a variety of approaches able to optimize the microstructural parameters with the aim to reach extreme performance in terms of strength, fracture toughness, penetration resistance, flexibility, but most of the previous studies do not take into account large deformations. Therefore, to the authors´ best knowledge, only few publications are available in the literature that address the investigation of the mechanical behavior of nacre-like composite materials in terms of instabilities at the microscopic as well as the macroscopic scale in a large deformation context.

In this work, we study the instability phenomena induced by uniaxial loading processes in bidimensional nacre-like composite microstructures made by incompressible hyperplastic materials. The interchange between the macroscopic and the microscopic instabilities in bioinspired composite materials has been investigated by examining different combinations of geometrical parameters (platelets volume fraction and platelets aspect ratio) and material parameters (shear modulus contrast between the platelets and the matrix). Comparing the microscopic and the macroscopic critical instability load factors evaluated in terms of critical stretch ratio, it has been obtained that the macroscopic behavior of nacre-like composite materials resulted to be strongly influenced by the material phase composition and the microscopic geometrical arrangement. Specifically, for a wide range of geometrical and material parameters, the obtained instabilities resulted to be global in nature with an in-phase mode shape, whereas the out-of-phase instability mode shapes occurred at a higher magnitude of the homogenized energy compared to the in-phase ones. The microscopic stability analysis provided high underestimates of the critical stretch ratios by adopting a small unit cell assembly, while it provides outcomes in line with the classical macroscopic stability analysis when it is performed by adopting a unit cell assembly with an appropriate size along the load direction. Definitively, the obtained results demonstrate that the macroscopic stability analyses performed on nacre-like composite materials, based on the classical criterion of the loss of strong ellipticity condition of the homogenized incremental moduli tensor, resulted more effective than a microscopic stability analysis involving larger unit cell assemblies. In addition, we found that, for a specific combination of geometrical and material parameters, nacre-like composite materials have shown local instabilities, requiring thus a full microscopic stability analysis.

2. Theoretical background

In this section, we summarize the background on the homogenization procedure and the stability conditions at the microscopic (section 2.1) and macroscopic (section 2.2) lengthscales. The analysis is further adopted for the nacre-like composite materials undergoing large deformations. Consider an RVE of a perfectly periodic nacre-like microstructure (see Fig. 1) characterized by an arbitrary assembly of the unit cells consisting of stiff platelets (reinforcement) interspaced with thin layers of soft material (matrix). As depicted in the figure on the left, the volume of the homogenized nacre-like solid is denoted by $\bar{V}_{(i)}$ (the subscript (i) is referred to variables in the undeformed configuration) and the surface enclosing the volume, on which the first Piola–Kirchhoff traction vector $\bar{\boldsymbol{t}}_R$ acts, is denoted by $\partial\bar{V}_{(i)}$. The undeformed and the deformed representative volume element (RVE) configurations are associated with an infinitesimal neighborhood of a generic point $\bar{\boldsymbol{X}}$ of the homogenized continuous body, and the macroscopic deformation gradient tensor is defined as $\bar{\boldsymbol{F}}$. With reference to the RVE, the microscopic gradient tensor is defined as $\boldsymbol{F} = \partial\boldsymbol{x}/\partial\boldsymbol{X}$, and the position vectors, corresponding to the undeformed (also identified as reference configuration) and the deformed configurations at the time t, are defined as $\boldsymbol{X}$ and $\boldsymbol{x}$, respectively. The volume change of the homogenized composite material with respect to the undeformed configuration is defined as $J \equiv \det\boldsymbol{F}$ and it represents the Jacobean of the transformation.

Let us consider a finitely deformed nacre-like composite material with nearly-incompressible neo-Hookean constituents characterized by a strain energy–density function $W(\boldsymbol{F})$. The equilibrium problem at the microscopic level is here formulated in terms of the deformation gradient tensor and its conjugated stress measure (the first-Piola Kirchhoff stress $\boldsymbol{T}_R$) since, as can be seen in the following, it leads to a simple definition of the essential boundary conditions on the RVE. The loading process can be parametrized in terms of a monotonically increasing time-like parameter $t \geq 0$; thus, by assuming a sufficiently small value of it, the incremental quantities can be considered as rate quantities. The microconstituents are characterized by the following incrementally linear relation:

$$\dot{\boldsymbol{T}}_R = \boldsymbol{C}^R[\dot{\boldsymbol{F}}], \tag{1}$$

where $\dot{\boldsymbol{T}}_R$ is the rate of the first-Piola Kirchhoff stress tensor, $\boldsymbol{C}^R$ is the fourth-order tensor of tangent moduli. The tensor enjoys the major symmetry condition $C^R_{ijhk} = C^R_{hkij}$, and $\dot{\boldsymbol{F}}$ is the rate of the deformation gradient tensor. The stress tensor $\boldsymbol{T}_R$ and the corresponding tangent moduli tensor $\boldsymbol{C}^R$ can be expressed as the first and the second derivative of the strain energy–density function, respectively as:

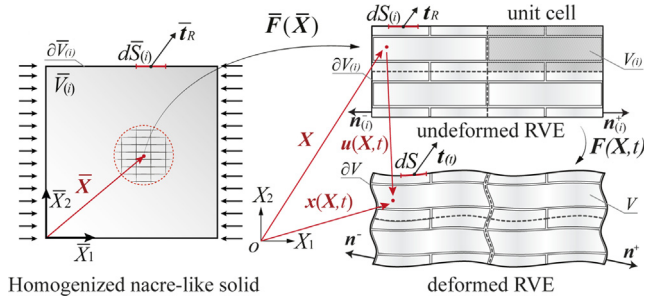

Fig. 1. Homogenized nacre-like solid material (to the left) and the corresponding undeformed and deformed representative volume element configurations (to the right) defined by a 2 × 2 unit cell assembly.

$$\boldsymbol{T}_R = \frac{\partial W}{\partial \boldsymbol{F}},\ \boldsymbol{C}_R = \frac{\partial^2 W}{\partial \boldsymbol{F}^2}. \tag{2}$$

Under the classical homogenization theory assumptions, the macroscopic constitutive response is based on an equilibrium state in which the volume forces are neglected and, as a consequence, the local stress field $\boldsymbol{T}_R(\boldsymbol{X})$ is divergence-free. Therefore, considering a quasi-static deformation process, the equation of the motion related to the undeformed configuration can be expressed in the following form:

$$\mathrm{Div}\boldsymbol{T}_R = \boldsymbol{0}. \tag{3}$$

The microscopic and the macroscopic scales are coupled by the following relations. The first defines the macroscopic first Piola-Kirchhoff stress tensor $\bar{\boldsymbol{T}}_R$ as a function of the traction field $\boldsymbol{t}_R$, and the second defines the macroscopic deformation gradient $\bar{\boldsymbol{F}}$ as a function of the deformation field $\boldsymbol{x}$:

$$\bar{\boldsymbol{T}}_R = \frac{1}{|V_{(i)}|}\int_{\partial V_{(i)}} \boldsymbol{t}_R \otimes \boldsymbol{X} dS_{(i)},\ \bar{\boldsymbol{F}} = \frac{1}{|V_{(i)}|}\int_{\partial V_{(i)}} \boldsymbol{x} \otimes \boldsymbol{n}_{(i)} dS_{(i)}, \tag{4}$$

where $\otimes$ denotes the tensor product, $\boldsymbol{t}_R = \boldsymbol{T}_R\boldsymbol{n}_{(i)}$ the first Piola–Kirchhoff traction vector, and $\boldsymbol{n}_{(i)}$ the outward normal at $\boldsymbol{X} \in \partial V_{(i)}$. The microscopic deformation field $\boldsymbol{x}$, expressed as a function of the macroscopic deformation gradient $\bar{\boldsymbol{F}}$, is assumed defined by the sum of a linear part, which represents the homogeneous deformations, and a correction part $\boldsymbol{w}$, also called fluctuation field:

$$\boldsymbol{x} = \bar{\boldsymbol{F}}\boldsymbol{X} + \boldsymbol{w}. \tag{5}$$

By replacing the microscopic deformation field (5) into the expression of the macroscopic deformation gradient $(4)_2$, it follows that the subsequent integral constraint has to be satisfied by the fluctuation field $\boldsymbol{w}$ to make the latter a kinematically admissible field:

$$\int_{\partial V_{(i)}} \boldsymbol{w} \otimes \boldsymbol{n}_{(i)} dS_{(i)} = \boldsymbol{0}. \tag{6}$$

Coherently with the periodic nature of the nacre-like microstructure, by ensuring a periodic distribution of the stress and strain field quantities which is compatible with the assumed periodic distribution of the geometrical and material properties, the integral constraint (6) can be satisfied, as in the following, by imposing periodic fluctuations on the RVE boundary $\partial V_{(i)}$:

$$\boldsymbol{w}(\boldsymbol{X}^+, t) = \boldsymbol{w}(\boldsymbol{X}^-, \mathrm{t}) \text{ on } \partial V_{(i)}, \tag{7}$$

where the superscripts + and – are referred to as pair of points placed on the opposite sides of the RVE boundaries. Such applied boundary conditions correspond to impose, from the viewpoint of deformation, a periodic deformation:

$$\boldsymbol{x}^+ - \boldsymbol{x}^- = \bar{\boldsymbol{F}}(\boldsymbol{X}^+ - \boldsymbol{X}^-) \text{ on } \partial V_{(i)}, \tag{8}$$

while, from the viewpoint of the equilibrium, they correspond to imposing antiperiodic tractions:

$$\left(\boldsymbol{T}_R\boldsymbol{n}_{(i)}\right)^+ = \left(-\boldsymbol{T}_R\boldsymbol{n}_{(i)}\right)^- \text{ on } \partial V_{(i)}. \tag{9}$$

Therefore, the nonlinear quasi-static boundary value problem (BVP) has been identified by the following relations:

$$\begin{cases} \mathrm{Div}\boldsymbol{T}_R = \boldsymbol{0} \text{ in } V_{(i)} \\ \left(\boldsymbol{T}_R\boldsymbol{n}_{(i)}\right)^+ = \left(-\boldsymbol{T}_R\boldsymbol{n}_{(i)}\right)^- \text{ on } \partial V_{(i)} \end{cases}. \tag{10}$$

The microstructural RVE boundary value problem is then solved by means of the finite element method in a variational framework:

$$\int_{V_{(i)}} T_R \cdot \nabla\delta\boldsymbol{w} dV_{(i)} = 0\ \forall\ \delta\boldsymbol{w} \in H^1\left(k^N V_{(i)\#}\right), \tag{11}$$

where $\boldsymbol{w}$ denotes the fluctuation solution at a given $\bar{\boldsymbol{F}}$ and $H^1(k^N V_{(i)\#})$ denotes the order one Hilbert space of vector-valued functions which are periodic over all possible unit cell assembly $k^N = [0,k]^N$, with k equal to an arbitrary integer and $N = 2$ for bidimensional problems.

The variational form defining the microscopic incremental equilibrium problem induced by an incremental change in the macroscopic deformation gradient $\dot{\bar{\boldsymbol{F}}}$ is characterized by the following variational form:

$$\int_{V_{(i)}} \boldsymbol{C}_R[\dot{\bar{\boldsymbol{F}}} + \nabla\dot{\boldsymbol{w}}] \cdot \nabla\delta\dot{\boldsymbol{w}} dV_{(i)} = 0\ \forall\ \delta\dot{\boldsymbol{w}} \in H^1(k^N V_{(i)\#}), \tag{12}$$

where $\dot{\boldsymbol{w}}$ denotes the incremental fluctuation field induced by $\dot{\bar{\boldsymbol{F}}}$. Once the variational problem (12) is solved, by virtue of the following relation:

$$\dot{\bar{\boldsymbol{T}}}_R = \bar{\boldsymbol{C}}^R[\dot{\bar{\boldsymbol{F}}}], \tag{13}$$

and by virtue of the fundamental identity $\dot{\bar{\boldsymbol{T}}}_R = \dot{\bar{\boldsymbol{T}}}_R$, it follows that the macroscopic constitutive response, written in terms of the homogenized tangent moduli tensor $\bar{\boldsymbol{C}}^R(\bar{\boldsymbol{F}})$, is determined by the following relation:

$$\bar{\boldsymbol{C}}^R_{ijhk}\left(\bar{\boldsymbol{F}}\right) = \frac{1}{|V_{(i)}|}\int_{V_{(i)}} C^R_{ijmn}\left(\boldsymbol{X}, \bar{\boldsymbol{F}}\right)\left[I^{hk}_{mn} + \nabla\dot{w}^{hk}_{mn}\right] dV_{(i)}$$

with $\dot{\boldsymbol{w}}^{hk}$ being the incremental fluctuation field induced by $\dot{\bar{\boldsymbol{F}}} = \boldsymbol{I}^{hk}$ and thus $I^{hk}_{mn} = \delta_{mh}\delta_{nk}$.

2.1. Macroscopic instability

The macroscopic stability analysis performed on a unit cell of a periodic heterogeneous material is based on its macroscopic properties. Specifically, the classical macroscopic stability measure was identified as the strong ellipticity condition of the homogenized tangent moduli tensor related to the unit cell:

$$\bar{\Lambda}(\bar{\boldsymbol{F}}(\lambda)) = \min_{||\boldsymbol{m}|| = ||\boldsymbol{n}|| = 1}\{\bar{\boldsymbol{C}}^R_0(\boldsymbol{m} \otimes \boldsymbol{n}) \cdot \boldsymbol{m} \otimes \boldsymbol{n}\} > 0, \tag{15}$$

in which the minimum is taken over all unit vectors $\boldsymbol{m}$ and $\boldsymbol{n}$, λ denotes the load parameter and $\bar{\boldsymbol{C}}^R_0$ denotes the fourth-order tensor of nominal instantaneous moduli that is defined by the following expression:

$$\bar{C}^R_{0ijhk} = \frac{1}{\det\boldsymbol{F}} F_{jm}F_{ln}\bar{C}^R_{imkn}. \tag{16}$$

The load factors associated with the classical macroscopic instability measure are defined as:

$$\begin{cases} \bar{\Lambda}(\bar{\lambda}_c) = 0 \\ \bar{\Lambda}(\bar{\lambda}) > 0\ \forall\ 0 \leqslant \bar{\lambda} < \bar{\lambda}_c \end{cases}, \tag{17}$$

where $\bar{\lambda}_c$ is the macroscopic critical load factor. Geymonat et al. [47] have demonstrated that in heterogeneous materials subjected to monotonic macroscopic loading, the onset of a primary instability can be

detected by means of a macroscopic stability analysis uniquely in the cases in which the instability mode shape is global (that is when the wavelength of the first instability is much larger than the unit cell size). In the case of instabilities characterized by wavelengths comparable with the unit cell size, the macroscopic stability condition still holds and the one-cell homogenized moduli tensor results to be still strongly elliptic.

2.2. Microscopic instability

The microscopic stability analysis is performed by superimposing at the microscopic scale an additional displacement field $\boldsymbol{u}(\boldsymbol{x},\tau)$ by taking the current equilibrium configuration as the reference one and assuming it as known. Such field is superimposed on the unit cell boundary ∂V satisfying the essential boundary conditions and deforming the unit cell from the current configuration $k^N V$ to the generic configuration $k^N V(\tau)$, where $\tau \geqslant 0$ denotes a time-like parameter. The incremental version of the classical stability criterion related to the current equilibrium configuration has been used to obtain the microscopic stability condition [48]. Greco and Luciano [33] considered the difference between the internal deformation work D and the work done by the anti-periodic traction vectors L, acting in the current configuration during the transformation from $k^N V$ to $k^N V(\tau)$. The microscopic structural stability condition of the examined unit cell at a given macroscopic deformation $\bar{\boldsymbol{F}}$ is identified by examining the sign of the following stability functional:

$$D - L = \left(\int_{k^N V} \dot{\boldsymbol{T}}_{R0} \cdot \boldsymbol{L} dV\right)\frac{t^2}{2} + o(t^2), \tag{18}$$

where $\dot{\boldsymbol{T}}_{R0}$ denotes the incremental form of the first Piola-Kirchhoff stress tensor evaluated in the configuration $k^N V = k^N V(\tau = 0)$. The incremental stress tensor can be expressed as:

$$\dot{\boldsymbol{T}}_{R0} = \boldsymbol{C}_0^R[\boldsymbol{L}] \tag{19}$$

where $\boldsymbol{L}$ is the gradient of the fluctuation field velocity:

$$\boldsymbol{L} = \nabla \dot{\boldsymbol{w}}(\boldsymbol{x}) \tag{20}$$

and definitively, the microscopic stability functional becomes:

$$\int_{k^N V} \boldsymbol{C}_0^R[\nabla \dot{\boldsymbol{w}}(\boldsymbol{x})] \cdot \nabla \dot{\boldsymbol{w}}(\boldsymbol{x})\, dV > 0 \tag{21}$$

Therefore, a given microstructure that is characterized by the fluctuation field $\boldsymbol{w}(\boldsymbol{x})$ induced by the macroscopic gradient deformation tensor $\bar{\boldsymbol{F}}$ results to be stable if the minimum eigenvalue of the stability functional (21) is positive if taken over all the admissible incremental periodic fluctuations on the $k^N V$ ensemble of unit cells:

$$\Lambda(\bar{\boldsymbol{F}}) = \inf_{k \in N}\left\{\min_{\dot{\boldsymbol{w}} \in H^1(k^N V \#)}\left\{\frac{\int_{k^N V} \boldsymbol{C}_0^R[\nabla \dot{\boldsymbol{w}}(\boldsymbol{x})] \cdot \nabla \dot{\boldsymbol{w}}(\boldsymbol{x})\, dV}{\int_{k^N V} \nabla \dot{\boldsymbol{w}}(\boldsymbol{x}) \cdot \nabla \dot{\boldsymbol{w}}(\dot{\boldsymbol{x}})\, dV}\right\}\right\} > 0. \tag{22}$$

3. Numerical results

The analyzed 2D unit cell (see Fig. 2) for the considered nacre-like composite microstructure, is composed by stiff platelets (grey areas) and a soft matrix (white areas) arranged in a brick and mortar pattern. The length and the height of the unit cell are denoted with L and H, respectively, and the amount of the stiff inclusions is defined by the volume fraction $v_f = (L_p H_p)/[(L_p + H_i)(H_p + H_i)]$, where L_p is the platelets length equal to 20 mm, H_p is the platelets height and H_i is the thickness of the matrix interphase. The platelets geometry is characterized by an aspect ratio $w = L_p/H_p$ and the constitutive law adopted to model the mechanical behavior of each microstructural phase (platelets and matrix) is the neo-Hookean hyperelastic, which is defined by the following energy density function:

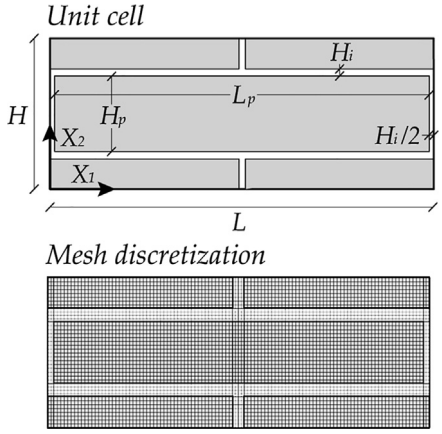

Fig. 2. Unit cell of the periodic nacre-like composite material in which the gray and white areas represent the stiff inclusions and the soft matrix interphase, respectively, together with an example of mesh discretization for the specific case with $v_f = 0.8$ and $w = 8$.

$$W_\xi = \frac{1}{2}\mu_\xi(\mathrm{tr}(C_\xi) - 3) - \mu_\xi \ln(J_\xi) + \frac{1}{2}\lambda_\xi \ln(J_\xi)^2 \tag{23}$$

where ξ stands for p or m when it refers to the platelets or the matrix, respectively, μ_ξ is the initial shear modulus, C_ξ is the right elastic Cauchy-Green tensor, J_ξ is the Jacobian of the 2D transformation and λ_ξ is the first Lamé parameter which governs the material compressibility.

The ratio between the initial shear modulus of the stiff platelets and the soft matrix is denoted as $k = \mu_p/\mu_m$ with μ_m equal to 20 MPa and to impose the incompressible behavior of the microstructural constituents λ_ξ has been fixed equal to $1000\mu_\xi$. The numerical analyses have been performed under plane strain conditions in a finite deformation framework, specifically, the nacre-like composite material has been subjected to a uniaxial macroscopic compression load along the X_1 direction which is imposed, in terms of the macroscopic deformation gradient tensor $\bar{\boldsymbol{F}}(\lambda)$, by means of the periodic boundary conditions applied on the external RVE boundaries. The corresponding macroscopic deformation gradient tensor assumes the following expression:

$$\bar{\boldsymbol{F}}(\bar{\lambda}) = \bar{\lambda}\boldsymbol{e}_1 \otimes \boldsymbol{e}_1 + \bar{\lambda}^{-1}\boldsymbol{e}_2 \otimes \boldsymbol{e}_2 \tag{24}$$

where $\bar{\lambda}$ represents the macroscopic stretch ratio in the X_1 direction that is equal to $(1 - \beta)$ with β defined as the load parameter, $\boldsymbol{e}_1$ and $\boldsymbol{e}_2$ are the unit basis vectors in the direction of X_1 and X_2, respectively. Note that the component of $\bar{\boldsymbol{F}}$ with reference to the direction X_2 is imposed equal to $\bar{\lambda}^{-1}$ with the aim to maintain the incompressibility condition during the uniaxial deformation process. A typical mesh discretization has been reported in Fig. 2 and it is composed of about 9000 quadratic Lagrangian quadrilateral elements that are mapped following a structured pattern. The number of mesh elements providing accurate results at the minimum computational effort has been obtained by performing a mesh convergence test for different values of volume fraction v_f, aspect ratio w, and shear modulus contrast k.

Fig. 3 shows the critical stretch ratios $\bar{\lambda}_c$ of the macroscopic instabilities for the lowest and the highest investigated values of k and w (i.e. $k = 20$, $k = 1000$ and $w = 0.1$, $w = 10$) and for v_f ranging from 0.1 to 0.9 with an increment of 0.1. In addition, with the aim to investigate the macroscopic instability behavior in the limit case of almost homogeneous materials, the values of v_f equal to 0.05 and 0.95 have been also investigated. From this figure it can be seen that 9000 quadratic elements are enough to obtain accurate results. The numerical simulations have been performed by employing the commercial software

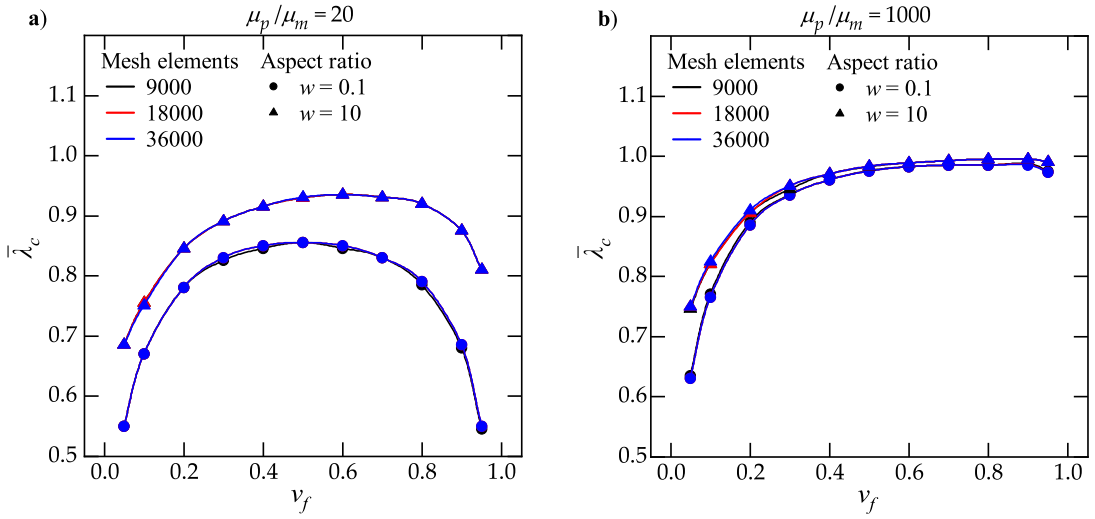

Fig. 3. Mesh sensitivity analysis of the macroscopic critical stretch ratio for different values of volume fraction (v_f), platelets aspect ratio (w) and shear modulus contrast $k = \mu_p/\mu_m = 20$ (a) and $k = 1000$ (b).

COMSOL MULTIPHISICS v5.5 together with two different subroutines written in the COMSOL Application Builder environment. The first one has been implemented to perform the macroscopic stability analysis and thus to evaluate, once the solution of the principal path is obtained, the homogenized tangent moduli tensor and, subsequently to evaluate the lowest eigenvalue associated with the acoustic tensor $\bar{\boldsymbol{Q}}_{0ih}(\bar{\boldsymbol{n}}) = \bar{C}^{R}_{0ijhk}\bar{n}_j\bar{n}_k$. The second one, instead, has been implemented to evaluate in a sequential way, for each loading step of the principal path, the minimum eigenvalue associated with the microscopic structural stability functional for an increasing assembly of unit cells in the X_1 direction, allowing to investigate the interplay between the instabilities with short and long wavelengths.

3.1. Macroscopic stability analysis

We start with determining the critical stretch ratios corresponding to the onset of elastic instability with long wavelength (macroscopic instabilities) in uniaxially compressed nacre-like composite materials. A comprehensive parametric analysis with respect to the main material and microstructural parameters (i.e., shear modulus contrast, platelets volume fraction, and platelets aspect ratio) has been carried out. Specifically, the shear modulus contrasts considered in the analysis are $k = 20$, 100, 500, and 1000, the investigated aspect ratios are equal to $w = 0.1$, 0.5, 1, 5, and 10, combining these parameters with a volume fraction v_f ranging from 0.1 to 0.9 with an increment of 0.1, and with v_f equal to 0.05 and 0.95 representing the limit cases of almost homogeneous material. To investigate the influence of the platelets volume fraction on the onset of macroscopic instabilities, in Fig. 4 the macroscopic instability curves have been reported as a function of the platelets volume fraction, for a wide range of aspect ratios w (i.e., $w = 0.1$, 0.5, 1, 5 and 10).

We observe that the critical stretch ratio has an increasing trend for low volume fractions until reaching a peak and then a decreasing trend for high volume fractions. The curves peaks have been denoted by the cross symbols, while the intersections between the black critical curves (corresponding to $w = 0.1$) and the red critical curves (corresponding to $w = 0.5$) are marked by the black dashed straight lines to easily identify the geometrical parameters giving the lowest critical stretch ratios. The nacre-like microstructures with a high shear modulus contrast (i.e., with $k = 500$ and $k = 1000$) experience macroscopic instabilities at lower uniaxial compressive loading (corresponding to higher critical stretch ratios). No significant differences have been observed in the instability critical curves by incrementing the initial shear modulus from 500 to 1000 (see Fig. 4c and d), thus in the following results, the highest analyzed shear modulus contrast is referred to k equal to 1000.

As can be seen in Fig. 4a, in the nacre-like materials with shear modulus contrast $k = 20$, the macroscopic instability critical curve peaks have been reached for intermediate values of volume fraction (i.e., $0.5 \leqslant v_f \leqslant 0.7$), while for the high value of $k = 1000$ (see Fig. 4d) the peaks are reached for higher volume fractions (i.e., $0.8 \leqslant v_f \leqslant 0.9$). For the cases with $k \leqslant 100$, low values of platelets volume fraction (i.e., $v_f \leqslant 0.5$) allow the composite to reach higher uniaxial deformations (as compared to those reached with high volume fractions) before the appearance of macroscopic instabilities, except for the case with $k = 20$ and $w = 0.1$ in which a symmetric trend of the critical stretch ratio with respect to $v_f = 0.5$ has been obtained. This behavior becomes more pronounced as initial shear modulus contrasts is increased. For example, for the cases with $k \geqslant 500$, the macroscopic instability curves show an increasing branch as the volume fraction increase until reaching a peak, and subsequently, they hold an almost constant value without starting a decreasing branch (see Fig. 4c and d).

Generally speaking, the nacre-like microstructures exhibit different macroscopic stability properties by varying the main geometrical parameters; in particular, with except of the curves with $w = 0.1$ the critical stretch ratio decreases with a decrease in the platelets aspect ratio with slight variations in the slopes depending on the value of the volume fraction adopted. Thus, for the case with $k = 20$ and $v_f = 0.05$ a percentage decreases of the critical stretch ratio of about 31% can be reached by decreasing the platelets aspect ratio from 10 to 1, while with the same value of shear modulus contrast and with the highest value of volume fraction (i.e., $v_f = 0.95$) a percentage decrease of about 12% can be reached. For an increasing shear modulus contrast, such as percentage decrease remains stable at about 30% for low platelets volume fractions, while it strongly decreases for high platelets volume fractions, reaching merely 1% for the case with $k = 1000$ and $v_f = 0.95$. As shown in Fig. 4, the highest critical stretch ratios have been obtained for a platelets aspect ratio w equal to 10 (blue curves), which indicates the destabilizing effect of high platelets aspect ratios, while the lowest critical stretch ratio has been obtained for w equal to 1 or 0.1 (depending on the value of the volume fraction) highlighting the stabilizing effect instead of low platelets aspect ratios.

To further elucidate the influence of the platelets aspect ratio w on the onset of macroscopic instabilities, in Fig. 5 the macroscopic insta-

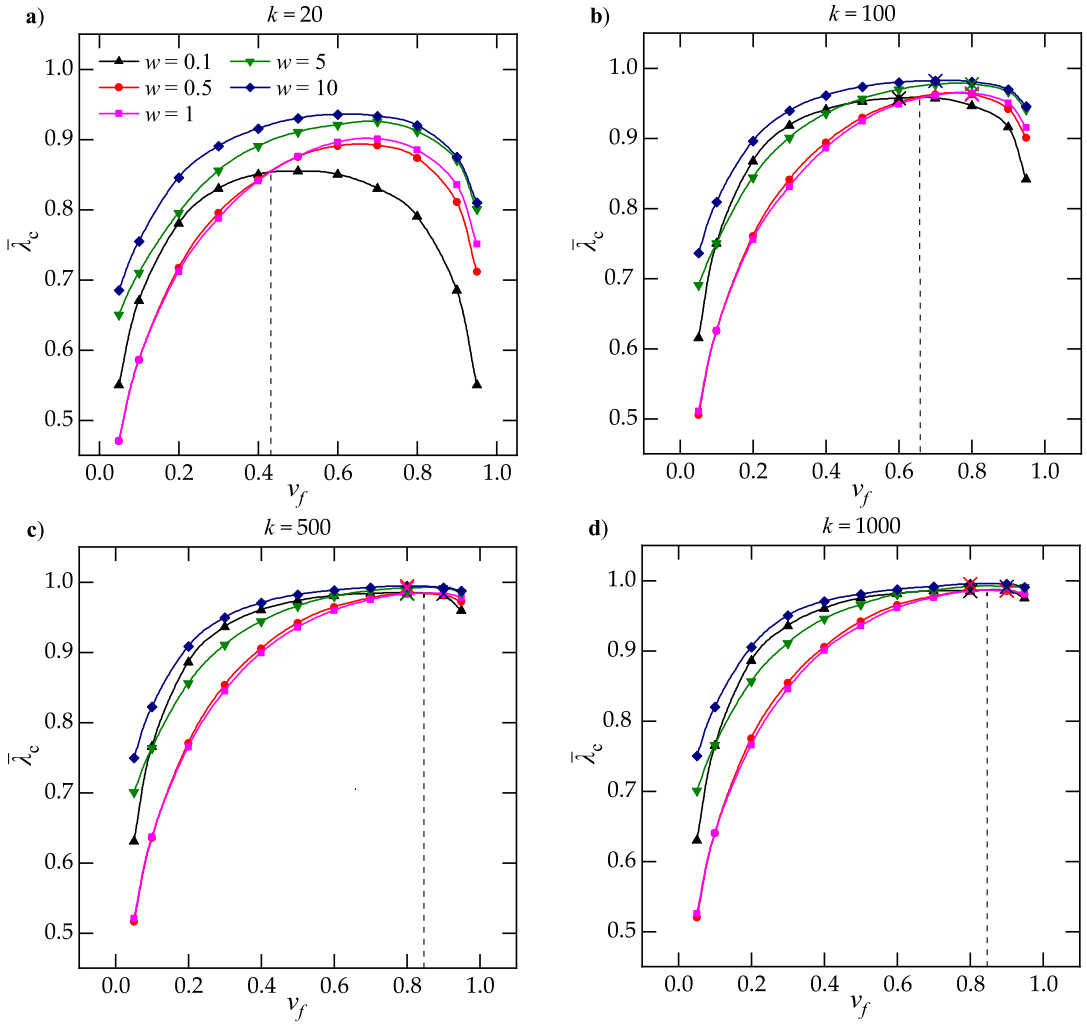

Fig. 4. Dependence of the macroscopic critical stretch ratio on the reinforcement volume fraction v_f (platelets) for nacre-like composite materials with different values of platelets aspect ratio w and shear modulus contrast equal to $k = 20$ (a), $k = 100$ (b), $k = 500$ (c) and $k = 1000$ (d).

bility curves has been reported as a function of the platelets aspect ratio w for a wide range of volume fractions v_f (i.e., $v_f = 0.05$, 0.1, 0.2, 0.3, 0.4, 0.5, 0.6, 0.7, 0.8, 0.9 and 0.95). We can observe that for the cases with a shear modulus contrast $k \leqslant 100$ (Fig. 5a and b) and platelets volume fractions $v_f \geqslant 0.6$, the critical stretch ratio increases as the platelets aspect ratio increases until reaching an almost zero slope for $w > 10$, while for platelets volume fractions $v_f < 0.6$ the critical curves show initially a decreasing branch until reaching a point of minimum for $0.5 \leqslant w \leqslant 1$ and then an increasing branch.

In addition, for the cases with a shear moduli contrast $k \geqslant 500$ (Fig. 4c and d), the critical instability curves related to a platelets volume fraction $v_f \geqslant 0.6$ increase only slightly as the aspect ratio increases (barely visible in the figure), maintaining very high values of the critical stretch ratios. While the critical instability curves related to a platelets volume fraction $v_f \leqslant 0.6$ show a similar trend to those obtained with $k \leqslant 100$, but they highlight higher values of the critical stretch ratios.

To further investigate the influence of the shear modulus contrast k on the onset of the macroscopic instabilities, in Fig. 6 the macroscopic instability curves has been reported as functions of the platelets volume fraction v_f for different values of k (i.e., $k = 20$, 100, 500 and 1000) and platelets aspect ratio equal to $w = 0.1$ (a), $w = 0.2$ (b), $w = 0.5$ (c), $w = 1$ (d), $w = 5$ (e) and $w = 10$ (f).

Consistent with the previous observation, we find no remarkable differences between the composites with shear modulus contrast k equal to 500 (red curve) and 1000 (black curve) for the considered range of the platelets volume fractions and aspect ratios. However, the change in the shear modulus contrast from $k = 20$ (blue curve) to 100 (magenta curve), results in a significant change of the critical stretch ratio. The critical stretch ratio decreases significantly as the stiffness ratio between the stiff platelets and the soft matrix is decreased.

By taking the critical stretch ratios obtained with a shear modulus contrast k equal to 1000 as the reference, the percentage decreases in the critical stretch ratios have been summarized in Table 1 for composites with varying shear modulus contrasts, platelets volume fractions, and platelets aspect ratios. Here we observe that despite the low values of the percentage changes obtained by decreasing the shear modulus contrast from 1000 to 500 (which are about 1%), the general trend of the percentage changes is decreasing as the shear modulus contrast decreases and as the platelets aspect ratio increases, thus, obtaining in some cases remarkable percentage changes. We note that in the composites with low shear modulus contrasts, the platelets can develop high deformations leading to a stabilizing effect. Similar behaviors have been reported in other composite materials, such as in soft composites with stiff circular inclusions periodically distributed [49], in compressible layered composites [50], and in 3D periodic fiber-reinforced composites [51]. The higher percentage changes have been obtained for high platelets volume fractions (i.e., $0.8 \leqslant v_f \leqslant 0.95$). This indicates that a change in the shear modulus contrast significantly

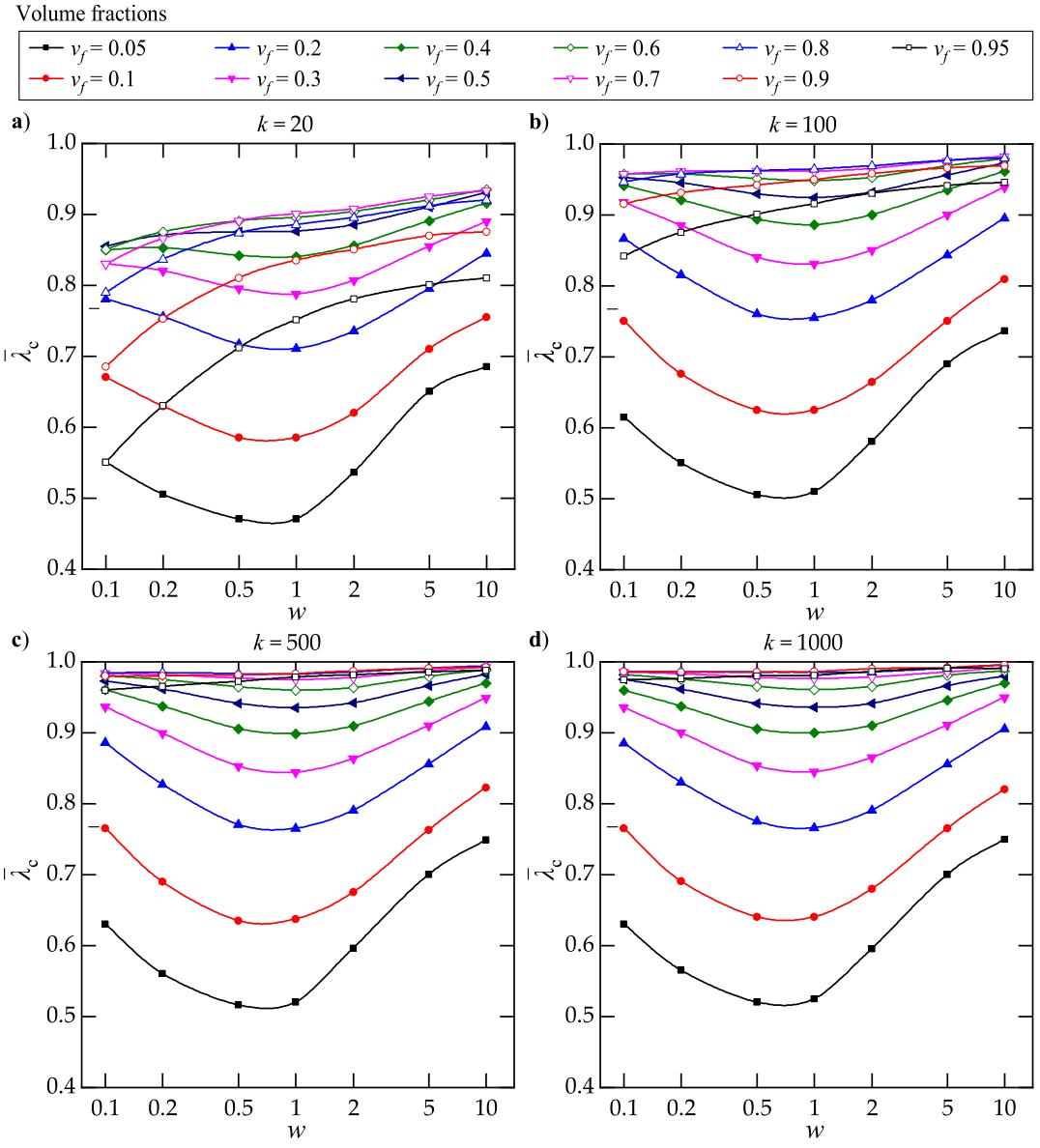

Fig. 5. Dependence of the macroscopic critical stretch ratio on the platelets aspect ratio w for nacre-like composite materials with different values of platelets volume fraction v_f and shear modulus contrast equal to $k = 20$ (a), $k = 100$ (b), $k = 500$ (c) and $k = 1000$ (d).

affects the critical stretch ratio in the composites with high volume fractions. The highest percentage decrease is 43.57%, which is obtained by decreasing the shear modulus contrast from 1000 to 20 in the composite with platelets aspect ratio 0.1 and platelets volume fraction 0.95.

3.2. Microscopic stability analysis

Here, by employing the microscopic stability analysis described in Section 2.2, the onset of microscopic instability in nacre-like composite materials subjected to uniaxial compression has been analyzed. To capture the domain size of the microscopic stability analysis in the case of a global instability mode, different assemblies of the considered unit cell have been evaluated.

We note that based on physical grounds supported by the numerical analysis reported in Fig. 7, for the investigated range of microstructure and material parameters, we exclude the onset of out-of-phase instability modes, so that, for the uniaxial macroscopic compression load along the X_1 direction considered here, it is sufficient considering only assemblies in the load direction, i.e. consisting of $n \times 1$ cells. In particular, the figure illustrates the first two instability modes for the composite characterized by a shear modulus contrast $k = 20$, platelets volume fraction $v_f = 0.5$, and platelets aspect ratio $w = 1$, by adopting an RVE assembly of $n \times 2$ cells with $n = 1, 2, 4, 8, 16, 32$ at a fixed stretch ratio λ coinciding with the macroscopic critical stretch ratio, i.e. $\lambda = \bar{\lambda}_c = 0.876$. Specifically, in Fig. 7a the trends of the first (lowest) and second eigenvalues, respectively denoted as Λ_1 and Λ_2 (both normalized with respect to the matrix shear modulus μ_p), are depicted by varying the RVE size in the X_1 direction. As can been seen in Fig. 7b, Λ_1 is related to the in-phase mode shape while Λ_2 is related to the out-of-phase mode shape. It is worth noting that the in-phase mode shape shows a one-cell periodicity in the X_2 direction.

Definitively, it can be seen that, at the microscopic scale, two characteristic failure modes may occur and that the stiff platelets can either show in-phase or out-of-phase instability modes. Comparing the trends of the related eigenvalues shown in Fig. 7a, we observe that the eigen-

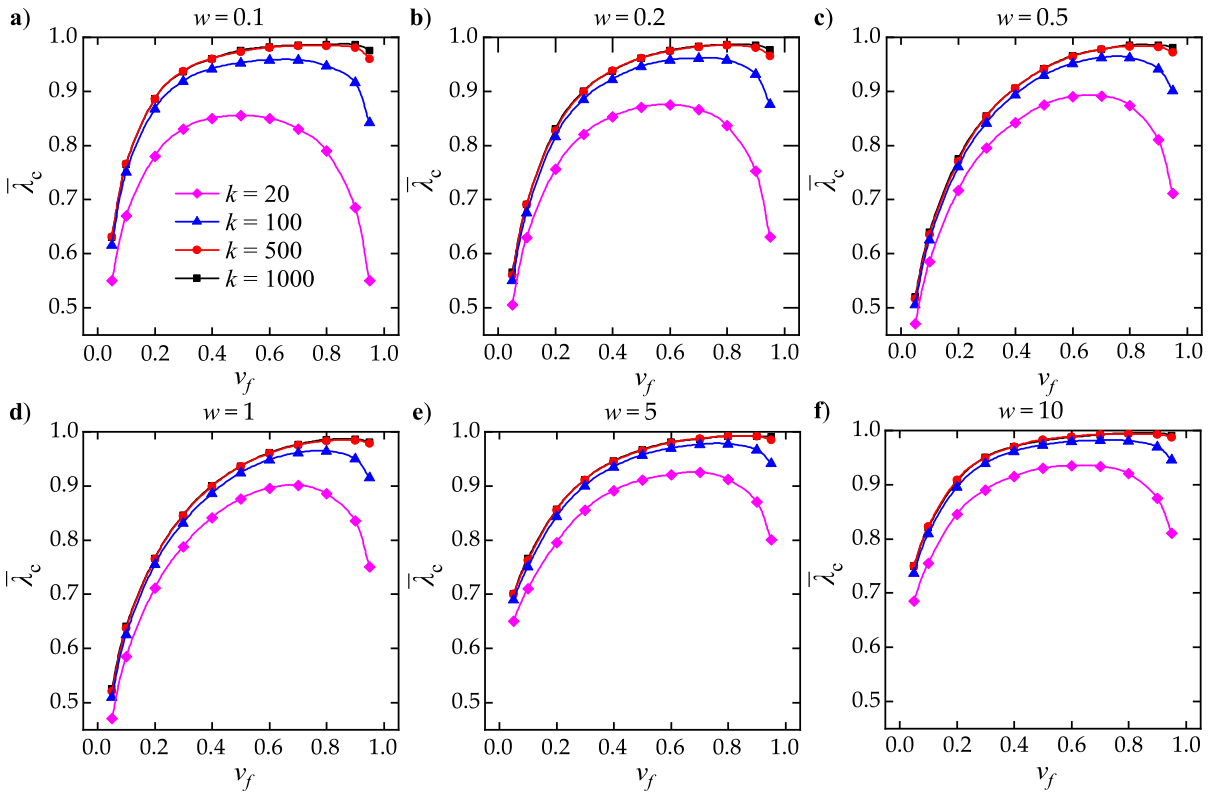

Fig. 6. Dependence of the macroscopic critical stretch ratio on the platelets volume fraction v_f for nacre-like composite materials with different values of shear modulus contrast k and platelets aspect ratio equal to $w = 0.1$ (a), $w = 0.2$ (b), $w = 0.5$ (c), $w = 1$ (d), $w = 5$ (e) and $w = 10$ (f).

Table 1
Percentage reductions in the critical stretch ratios by varying the shear modulus contrast k, aspect ratio w and volume fraction v_f and by taking as reference value the critical stretch ratio obtained for a shear modulus contrast equal to 1000.

		v_f 0.05	0.1	0.2	0.3	0.4	0.5	0.6	0.7	0.8	0.9	0.95
Reference values		0.630	0.765	0.886	0.935	0.960	0.975	0.981	0.985	0.986	0.986	0.975
w = 0.1	**k = 500**	0.03%	0.04%	0.02%	0.11%	0.01%	0.19%	0.09%	0.16%	0.20%	0.60%	1.57%
	k = 100	2.39%	1.95%	2.11%	1.85%	1.97%	2.31%	2.44%	2.85%	4.01%	7.14%	13.65%
	k = 20	12.70%	12.39%	11.87%	11.26%	11.46%	12.31%	13.36%	15.74%	19.88%	30.53%	43.57%
Reference values		0.565	0.691	0.830	0.900	0.937	0.961	0.975	0.983	0.986	0.985	0.976
w = 0.2	**k = 500**	0.85%	0.09%	0.36%	0.11%	0.07%	0.03%	0.08%	0.16%	0.21%	0.54%	1.09%
	k = 100	2.69%	2.18%	1.79%	1.67%	1.70%	1.67%	1.83%	2.18%	2.96%	5.51%	10.30%
	k = 20	10.57%	8.86%	8.99%	8.86%	8.98%	9.47%	10.25%	11.90%	15.17%	23.57%	35.39%
Reference values		0.520	0.640	0.775	0.854	0.905	0.941	0.965	0.977	0.985	0.985	0.980
w = 0.5	**k = 500**	0.79%	0.78%	0.62%	0.06%	0.02%	0.01%	0.11%	0.02%	0.22%	0.39%	0.82%
	k = 100	2.87%	2.32%	1.90%	1.51%	1.30%	1.27%	1.45%	1.56%	2.33%	4.40%	8.14%
	k = 20	9.57%	8.52%	7.52%	6.84%	7.00%	7.04%	7.73%	8.86%	11.34%	17.76%	27.40%
Reference values		0.525	0.640	0.766	0.845	0.900	0.936	0.961	0.976	0.985	0.986	0.981
w = 1	**k = 500**	0.89%	0.51%	0.09%	0.11%	0.17%	0.04%	0.11%	0.12%	0.25%	0.25%	0.27%
	k = 100	2.83%	2.34%	1.38%	1.70%	1.58%	1.22%	1.28%	1.48%	2.12%	3.62%	6.69%
	k = 20	10.40%	8.56%	7.12%	6.82%	6.63%	6.42%	6.77%	7.69%	10.14%	15.28%	23.41%
Reference values		0.700	0.765	0.856	0.911	0.945	0.966	0.980	0.986	0.991	0.991	0.990
w = 5	**k = 500**	0.01%	0.30%	0.05%	0.05%	0.13%	0.03%	0.12%	0.16%	0.02%	0.04%	0.53%
	k = 100	1.46%	1.97%	1.46%	1.15%	1.07%	1.01%	1.13%	0.97%	1.41%	2.55%	5.01%
	k = 20	7.15%	7.22%	7.08%	6.08%	5.79%	5.75%	6.11%	6.14%	8.03%	12.23%	19.16%
Reference values		0.750	0.820	0.905	0.950	0.970	0.980	0.987	0.991	0.995	0.995	0.990
w = 10	**k = 500**	0.13%	0.25%	0.33%	0.10%	0.00%	0.20%	0.10%	0.08%	0.12%	0.28%	0.28%
	k = 100	1.86%	1.35%	1.05%	1.14%	0.91%	0.73%	0.79%	0.95%	1.49%	2.58%	4.49%
	k = 20	8.67%	7.94%	6.64%	6.29%	5.66%	5.12%	5.27%	5.88%	7.54%	12.05%	18.19%

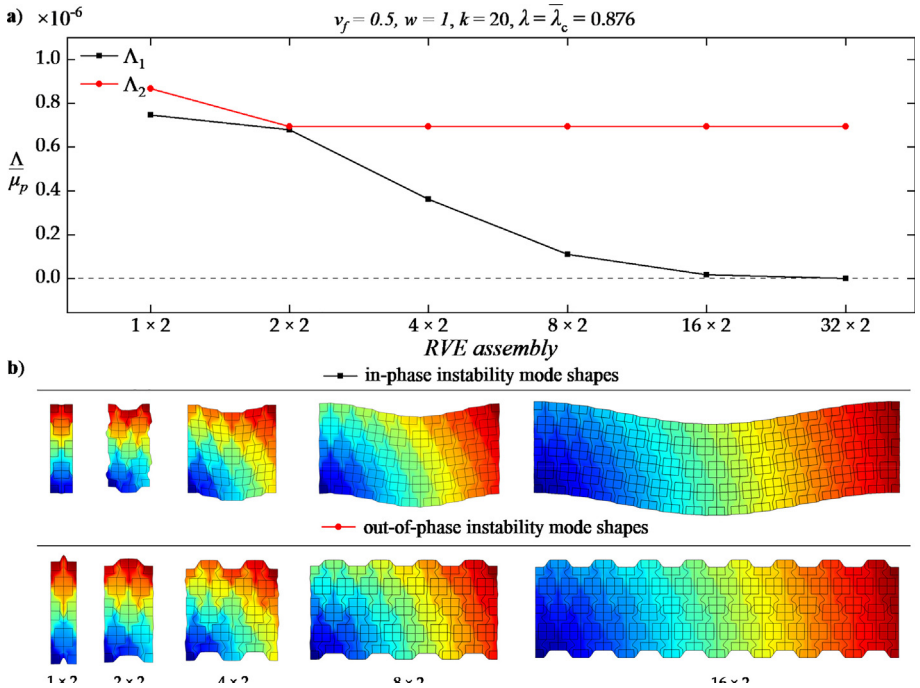

Fig. 7. First two normalized eigenvalues (associated with the in-phase and out-of-phase instability mode shapes) obtained for the microscopic stability problem, versus the size of the RVE assembly in the X_1 direction (a), and related critical mode shapes (b).

Table 2
Comparison between the macroscopic critical stretch ratios (reported as ref. value in the table) and microscopic critical stretch ratios obtained for an increasing unit cell assembly in composites with shear modulus contrast $k = 20$ together with the corresponding percentage changes.

			Unit cell assembly						
$k = 20$			1 × 1	2 × 1	4 × 1	8 × 1	16 × 1	32 × 1	64 × 1
$w = 0.1$	$v_f = 0.1$	λ_c	0.361	0.361	0.425	0.612	0.660	**0.672**	**0.674**
		ref. value	0.670						
		% change	−46.18%	−46.18%	−36.64%	−8.68%	−1.55%	**0.22%**	**0.62%**
	$v_f = 0.5$	λ_c	0.518	0.520	0.564	0.670	0.779	0.832	**0.848**
		ref. value	0.855						
		% change	−39.42%	−39.17%	−34.01%	−21.58%	−8.90%	−2.72%	**−0.77%**
	$v_f = 0.9$	λ_c	0.392	0.546	0.564	0.564	0.564	0.591	0.637
		ref. value	0.685						
		% change	−42.83%	−20.26%	−17.67%	−17.71%	−17.60%	−13.66%	−7.08%
$w = 1$	$v_f = 0.1$	λ_c	0.414	0.546	0.574	**0.585**	**0.585**	–	–
		ref. value	0.585						
		% change	−29.29%	−6.80%	−1.97%	**−0.02%**	**−0.03%**	–	–
	$v_f = 0.5$	λ_c	0.515	0.750	0.828	0.865	**0.874**	–	–
		ref. value	0.876						
		% change	−41.18%	−14.37%	−5.41%	−1.27%	**−0.14%**	–	–
	$v_f = 0.9$	λ_c	0.535	0.628	0.744	0.810	**0.829**	–	–
		ref. value	0.835						
		% change	−35.93%	−24.84%	−10.86%	−3.02%	**−0.77%**	–	–
$w = 10$	$v_f = 0.1$	λ_c	**0.756**	**0.758**	**0.758**	**0.758**	**0.758**	–	–
		ref. value	**0.755**						
		% change	**0.11%**	**0.35%**	**0.35%**	**0.35%**	**0.35%**	–	–
	$v_f = 0.5$	λ_c	0.913	**0.925**	**0.930**	**0.930**	**0.930**	–	–
		ref. value	0.93002						
		% change	−1.84%	**−0.51%**	**0.02%**	**0.02%**	**0.02%**	–	–
	$v_f = 0.9$	λ_c	0.851	**0.871**	**0.876**	**0.878**	**0.878**	–	–
		ref. value	0.87508						
		% change	−2.75%	**−0.46%**	**0.11%**	**0.30%**	**0.33%**	–	–

value Λ_2 associated with the out-of-phase instabilities (red curve) does not converge to 0, and that an in-phase critical mode shape should occur at the first onset of the instability (black curve). Therefore, the most relevant critical mode in the considered nacre-like microstructure (subjected to uniaxial compression) is the in-phase instability mode, as depicted in Fig. 7. This behavior is similar to that reported for the fiber-reinforced heterogeneous materials [32], indicating that the out-of-phase instability modes occur at a significantly higher magnitude of homogenized energy than the in-phase ones. In the light of such results, in the next numerical analyses we use only a single unit cell in the X_2 direction while varying the number of unit cells in the loading direction X_1. This allows us to reduce the computational effort of the numerical analysis by limiting the investigations to a single row of unit cells. Therefore, the microscopic stability analysis has been performed on nacre-like composite materials with increasing RVE size in the X_1 direction. The microscopic geometrical and material parameters are $v_f = 0.1$, 0.5, and 0.9, $w = 0.1$, 1 and 10, and shear modulus contrast $k = 20$, 100, and 1000. The obtained microscopic critical stretch ratios are summarized in Tables 2–4 for each investigated unit cell assembly to compare the macroscopic critical factors with the microscopic ones. In addition, to investigate the convergence of the microscopic critical load factors to the macroscopic ones at increasing RVE size, the percentage changes between the microscopic and the macroscopic critical stretch ratios (previously evaluated in section 3.1) have been evaluated. The assemblies with an increased number of unit cells show the predictions of the microscopic instability critical loads approaching the macroscopic ones. Moreover, the convergence between these predictions occurs with a relative tolerance of less than 1% being the assumed convergence threshold (the critical load values for which the convergence is reached have been highlighted in bold in the tables). It is important to note that, once the convergence of the predictions is achieved, the values of the percentage oscillate around the zero value, often changing their sign. This is due to the error related to the FE discretization and the error related to the linear interpolation method adopted to evaluate the critical stretch ratio. Table 2 summarizes the microscopic critical stretch ratios for a nacre-like microstructure with shear modulus contrast $k = 20$. Among the examined unit cell assemblies, the critical stretch ratio is underestimated by the microscopic critical stretch ratio compared to the macroscopic one (reported in the table as ref. value). The largest difference in the predictions is about 46.18% for the microscopic stability analyses performed on the 1×1 unit cell assemblies with $w = 0.1$ and 1. This is due to the fact that for nacre-like microstructures, the critical instability modes are global and thus, an RVE with a significantly large number of unit cells in the loading direction of the load is required to capture the global instability mode. Similar differences have been obtained for the cases with $k = 100$ and $w = 0.1$ (see Table 3). The results highlight that the difference in the predicted critical load decreases as the platelets aspect ratio w and the shear modulus contrast k increase. For nacre-like microstructures with $k = 1000$ (whose microscopic critical load factors are summarized in Table 4), significantly smaller differences have been obtained (no more than 4%).

We note that composites with platelets aspect ratio $w = 10$ show the prediction difference of the instability critical loads lower than 3%. This is regardless of the values of the platelets volume fraction and shear modulus contrast. As can be seen in Tables 2–4 the microscopic critical stretch ratios approach to the macroscopic ones from below leading to negative percentage changes with the except of the case reported in Fig. 8 in which the primary instability mode is of local type and, thus, the microscopic critical stretch ratio approaches to the macroscopic one from the above with positive percentage changes.

Table 3
Comparison between the macroscopic critical stretch ratios (reported as ref. value in the table) and microscopic critical stretch ratios obtained for an increasing unit cell assembly in composites with shear modulus contrast $k = 100$ together with the corresponding percentage changes.

			Unit cell assembly						
$k = 100$			1×1	2×1	4×1	8×1	16×1	32×1	64×1
$w = 0.1$	$v_f = 0.1$	λ_c	0.435	0.439	0.652	0.716	**0.744**	**0.751**	–
		ref. value	0.750						
		% change	−42.01%	−41.47%	−13.02%	−4.49%	**−0.77%**	**0.19%**	–
	$v_f = 0.5$	λ_c	0.504	0.666	0.766	0.861	0.917	**0.949**	–
		ref. value	0.953						
		% change	−47.12%	−30.07%	−19.56%	−9.66%	−3.75%	**−0.34%**	–
	$v_f = 0.9$	λ_c	0.837	0.835	0.835	0.836	0.836	0.881	0.898
		ref. value	0.916						
		% change	−8.64%	−8.76%	−8.76%	−8.65%	−8.70%	−3.79%	−1.89%
$w = 1$	$v_f = 0.1$	λ_c	0.450	0.586	0.615	**0.626**	**0.626**	–	–
		ref. value	0.625						
		% change	−27.97%	−6.23%	−1.65%	**0.17%**	**0.13%**	–	–
	$v_f = 0.5$	λ_c	0.692	0.825	0.886	**0.915**	**0.923**	**0.925**	–
		ref. value	0.924						
		% change	−25.16%	−10.74%	−4.09%	**−0.99%**	**−0.14%**	**0.07%**	–
	$v_f = 0.9$	λ_c	0.672	0.780	0.866	0.922	**0.943**	**0.950**	**0.952**
		ref. value	0.950						
		% change	−29.27%	−17.87%	−8.89%	−2.90%	**−0.74%**	**0.03%**	**0.16%**
$w = 10$	$v_f = 0.1$	λ_c	0.788	0.798	**0.806**	**0.809**	**0.810**	–	–
		ref. value	0.809						
		% change	−2.60%	−1.34%	**−0.32%**	**0.05%**	**0.16%**	–	–
	$v_f = 0.5$	λ_c	0.945	0.963	**0.971**	**0.973**	**0.973**	–	–
		ref. value	0.973						
		% change	−2.84%	−1.03%	**−0.24%**	**−0.02%**	**0.01%**	–	–
	$v_f = 0.9$	λ_c	0.941	**0.962**	**0.968**	**0.969**	–	–	–
		ref. value	0.969						
		% change	−2.90%	**−0.72%**	**−0.14%**	**−0.03%**	–	–	–

Table 4
Comparison between the macroscopic critical stretch ratios (reported as ref. value in the table) and microscopic critical stretch ratios obtained for an increasing unit cell assembly in composites with shear modulus contrast $k = 1000$ together with the corresponding percentage changes.

			Unit cell assembly						
$k = 1000$			1 × 1	2 × 1	4 × 1	8 × 1	16 × 1	32 × 1	64 × 1
$w = 0.1$	$v_f = 0.1$	λ_c	0.747	0.745	0.745	0.758	**0.768**	–	–
		ref. value	0.765						
		% change	−2.30%	−2.59%	−2.60%	**−0.97%**	**0.39%**	–	–
	$v_f = 0.5$	λ_c	0.938	0.935	0.935	0.940	**0.970**	–	–
		ref. value	0.975						
		% change	−3.77%	−4.07%	−4.07%	−3.57%	**−0.55%**	–	–
	$v_f = 0.9$	λ_c	0.975	0.975	0.975	0.975	0.975	0.975	**0.977**
		ref. value	0.986						
		% change	−1.12%	−1.12%	−1.12%	−1.12%	−1.12%	−1.12%	**−0.92%**
$w = 1$	$v_f = 0.1$	λ_c	0.616	0.618	0.633	**0.645**	**0.648**	–	–
		ref. value	0.640						
		% change	−3.77%	−3.51%	−1.13%	**0.79%**	**1.16%**	–	–
	$v_f = 0.5$	λ_c	0.908	0.906	0.913	**0.931**	**0.932**	–	–
		ref. value	0.936						
		% change	−2.97%	−3.12%	−2.46%	**−0.54%**	**−0.43%**	–	–
	$v_f = 0.9$	λ_c	0.960	0.960	0.960	0.964	**0.982**	**0.987**	**0.989**
		ref. value	0.986						
		% change	−2.58%	−2.58%	−2.58%	−2.22%	**−0.40%**	**0.11%**	**0.29%**
$w = 10$	$v_f = 0.1$	λ_c	0.809	0.812	**0.821**	**0.822**	**0.824**	–	–
		ref. value	0.820						
		% change	−1.35%	−1.03%	**0.12%**	**0.29%**	**0.52%**	–	–
	$v_f = 0.5$	λ_c	0.957	0.962	0.962	**0.981**	**0.983**	**0.984**	–
		ref. value	0.980						
		% change	−2.40%	−1.87%	−1.87%	**0.08%**	**0.31%**	**0.36%**	–
	$v_f = 0.9$	λ_c	0.965	**0.987**	**0.994**	**0.995**	**0.996**	–	–
		ref. value	0.995						
		% change	−2.97%	**−0.77%**	**−0.15%**	**0.01%**	**0.05%**	–	–

The geometrical and the material parameters combination for which the critical mode shape is local is given by $k = 20$, $v_f = 0.1$, $w = 10$. In this case, the percentage change is positive and, the onset of the local instability precedes the macroscopic loss of strong ellipticity. The related percentage variation is not significant, meaning that for this specific microstructure the macroscopic stability condition provides a good estimate of the primary instability, even if of local type. However, in the presence of different combinations of geometrical and material parameters, it is expected that the macroscopic stability analysis could lead to a more strongly unconservative prediction of the critical stretch ratio (namely, a larger value of the critical load factor is provided) with respect to a rigorous microscopic stability analysis. As can be seen in Fig. 8, the microscopic instability mode is characterized by a finite wavelength with the periodicity corresponding to a 2×1 unit cell assembly.

The results reported in Tables 2–4 also show that different convergence speeds can be obtained by varying the microstructure and the material parameters. Specifically, for the cases with low platelets aspect ratio (i.e., $w = 0.1$), the convergence speed increase as the shear modulus contrast increases. Fig. 9 illustrates this observation showing the critical mode shapes for the composites with identical microstructure parameters and varying shear modulus contrasts and the unit cell assembly. In Fig. 9a, the convergence between the microscopic and the macroscopic critical stretch ratios is reached by adopting unit cell assemblies $n \times 1$ with $n \geqslant 32$; while in Figs. 9b and c the convergence is faster, and it is reached by adopting $n \geqslant 16$ and $n \geqslant 8$, respectively.

On the other hand, for the cases with high platelets aspect ratio $w = 10$ the convergence speed decrease as the shear modulus contrast increases. However, for the cases with intermediate values of platelets aspect ratio $w = 1$ the convergence speed is not significantly influenced by the other geometrical and material parameters. The combination of microstructure parameters for which the critical instability modes is characterized by the longest wavelength (regardless of the

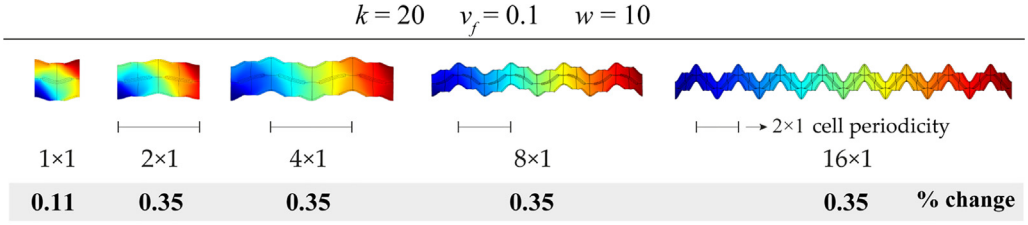

Fig. 8. Critical mode shapes exhibiting a local instability at increasing RVE size in the X_1 direction for a nacre-like microstructure with platelets volume fraction $v_f = 0.1$, platelets aspect ratio $w = 10$ and shear modulus $k = 20$.

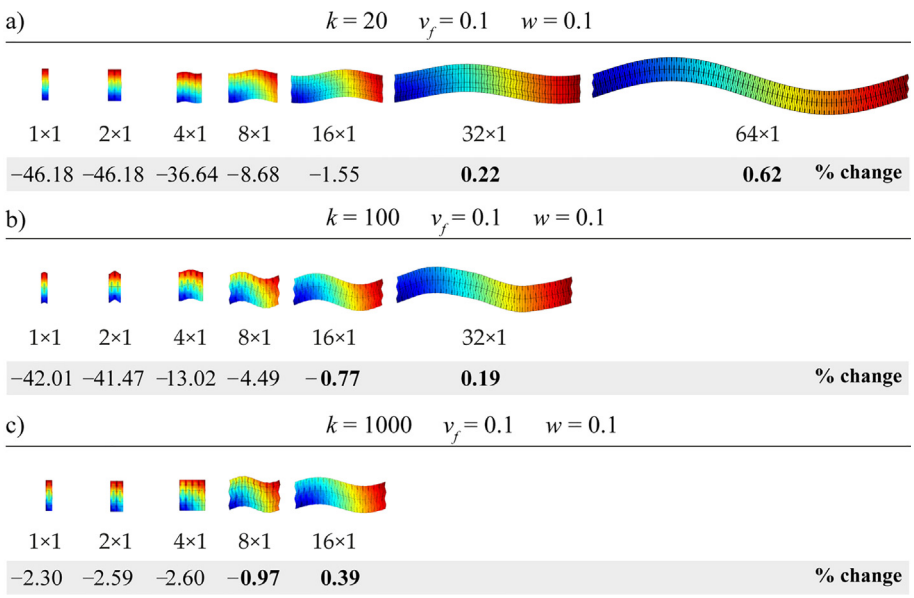

Fig. 9. Critical instability mode shapes at increasing RVE size in the X_1 direction for a nacre-like microstructure with platelets volume fraction $v_f = 0.1$, platelets aspect ratio $w = 0.1$ and shear modulus $k = 20$ (a), $k = 100$ (b) and $k = 1000$ (c).

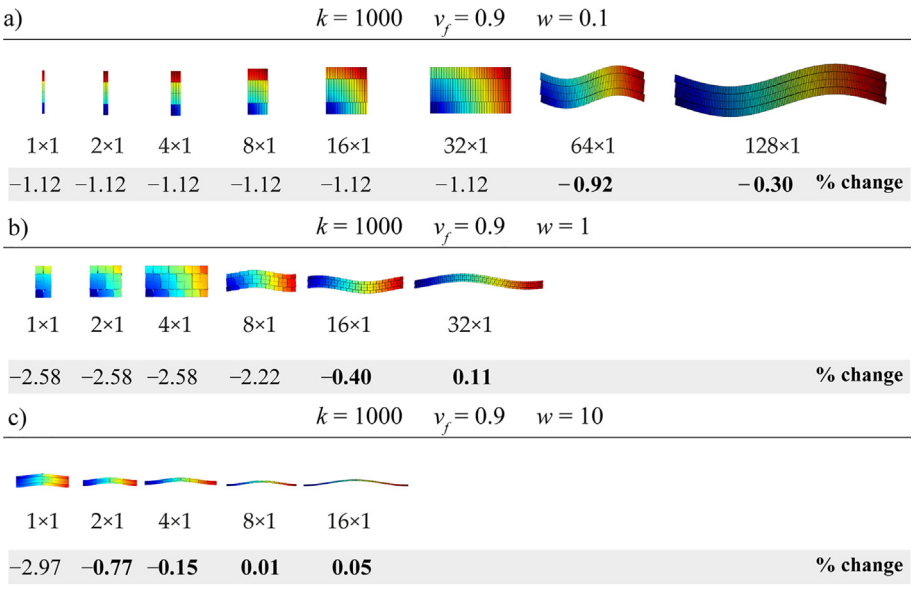

Fig. 10. Critical instability mode shapes at increasing RVE size in the X_1 direction for a nacre-like microstructure with shear modulus $k = 1000$, platelets volume fraction $v_f = 0.9$, and platelets aspect ratio $w = 0.1$ (a), $w = 1$ (b) and $w = 10$ (c).

shear modulus contrast) is $v_f = 0.9$ and $w = 0.1$ (see Fig. 10). In this case, a considerable number of unit cells in the X_1 direction is needed to capture the onset of the global instability by means of a microscopic stability analysis. For instance, in the case of a unit cell assembly 64×1 is needed to achieve the convergence between the microscopic and macroscopic critical stretch ratios highlighting thus that, by increasing the platelets aspect ratio, the critical instability wavelength can be reduced and, consequently, the convergence speed is increased. Definitively, for the investigated range of geometrical and material parameters, we found that the macroscopic stability analysis resulted to be more effective than the microscopic one to detect the onset of instabilities in nacre-like composite materials subjected to uniaxial loads in a large deformation context because, in many cases, the primary instabilities were of global type. On the other hand, we found that the combination of geometrical and material parameters characterized by high values of platelets aspect ratio and low values of platelets volume fraction and shear moduli contrast requires a full microscopic stability analysis since the local instability precedes the global one.

4. Conclusions

The present work deals with the stability analysis at both the microscopic and the macroscopic scale of 2D bioinspired incompressible composite materials characterized by a nacre-like microstructure and subjected to uniaxial loading processes in a finite-strain framework. The microscopic and the macroscopic instabilities have been

investigated by examining different combinations of platelets volume fraction, aspect ratio and shear modulus contrast between platelets and matrix phase. The macroscopic stability analyses were performed by employing the classical macroscopic stability condition (coinciding with the strong ellipticity condition of the homogenized tangent moduli tensor), and the related results have been reported in terms of the critical stretch ratios corresponding to the onset of elastic instabilities with long wavelengths. The results highlighted that the critical stretch ratios and the instability mode shapes, resulted to be highly influenced by both microscopic geometrical arrangement and material composition. Specifically, we can observe that the critical stretch ratios have an increasing trend for low volume fractions, until reaching a peak, and then a decreasing trend. The shear modulus contrast between the reinforcement platelets and the matrix represents an important material parameter influencing the instability phenomena in nacre-like composite materials. In the range of low shear modulus contrast it acts as weak stabilizing factor while, in the range of high shear modulus contrast it acts as an unstabilizing factor that leads thus to macroscopic instabilities at lower uniaxial compressive loading. In addition, has been highlighted that a change in the shear modulus contrast has a more significant effect on the critical stretch ratio in nacre-like microstructures with high volume fractions since, for instance, the highest percentage decrease of the critical stretch ratio (equal to 43.57%) has obtained by decreasing the shear modulus contrast from 1000 to 20 in the case with platelets aspect ratio equal to 0.1 and platelets volume fraction equal to 0.95. Next, the microscopic instabilities have been investigated by superimposing to an RVE of nacre-like composite material (defined by a single unit cell or an ensemble of cells) a perturbation of the equilibrium fluctuation field in the current configuration. We have found that for a wide range of geometrical and material parameters, the instabilities resulted to be characterized by long wavelengths with an in-phase mode shape and it has been also proved that the out-of-phase instability mode shapes occur at a significantly higher magnitude of the homogenized energy compared to the in-phase ones. We also observed that by adopting a small unit cell assembly, the microscopic stability analyses provide strong underestimates of the critical stretch ratios, while they provide similar results at the macroscopic stability analyses when they are performed by adopting large unit cell assemblies with prevalent dimension in the load direction. Just in one combination of the investigated geometrical and material parameters the critical mode shape resulted to be local and, in this case, the onset of the local instability precedes the macroscopic loss of strong ellipticity. Definitively, the obtained results have proved that the stability analyses performed on nacre-like composite materials subjected to uniaxial deformation in a large deformation context, can be based on the criterion of the loss of strong ellipticity condition of the homogenized incremental moduli tensor which is computationally less expensive than a microscopic stability analysis performed on a very large assembly of unit cells and that only a few microstructural morphologies, characterized in particular by low values of platelets volume fraction and shear moduli contrast together with high values of platelets aspect ratio, require a full microscopic analysis. However, also in such cases, the macroscopic stability analysis is able to provide reasonable estimate of the critical load factor.

Declaration of Competing Interest

The authors declare that they have no known competing financial interests or personal relationships that could have appeared to influence the work reported in this paper.

Acknowledgements

Fabrizio Greco gratefully acknowledges financial support from the Italian Ministry of Education, University and Research (MIUR) under the P.R.I.N. 2017 National Grant “Multiscale Innovative Materials and Structures” (Project Code 2017J4EAYB; University of Calabria Research Unit). Andrea Pranno gratefully acknowledges financial support from the Italian Ministry of Education, University and Research (MIUR) under the POR Calabria FESR-FSE 2014-2020, Rep. N. 1006 of 30/03/2018, Line B, Action 10.5.12. Stephan Rudykh gratefully acknowledges the financial support of Grainger Institute for Engineering and the University of Wisconsin Madison.

References

[1] Goshkoderia A, Arora N, Slesarenko V, Li J, Chen V, Juhl A, et al. Tunable permittivity in dielectric elastomer composites under finite strains: Periodicity, randomness, and instabilities. Int. J. Mech. Sci. 2020;186:105880. https://doi.org/10.1016/j.ijmecsci.2020.105880.

[2] Lima AVNA, Cardoso JL, Lobo CJS. Research on hybrid sisal/glass composites: A review. J. Reinf. Plast. Compos. 2019;38(17):789–821. https://doi.org/10.1177/0731684419847272.

[3] Zhang J, Dui G, Wang X. Post-micro-buckling of carbon fibers in functionally graded plates under pure bending. Eur. J. Mech. - ASolids. 2019;75:419–25. https://doi.org/10.1016/j.euromechsol.2019.02.007.

[4] Goshkoderia A, Chen V, Li J, Juhl A, Buskohl P, Rudykh S. Instability-Induced Pattern Formations in Soft Magnetoactive Composites. Phys. Rev. Lett. 2020;124(15). https://doi.org/10.1103/PhysRevLett.124.158002.

[5] Slesarenko V, Volokh KY, Aboudi J, Rudykh S. Understanding the strength of bioinspired soft composites. Int. J. Mech. Sci. 2017;131–132:171–8. https://doi.org/10.1016/j.ijmecsci.2017.06.054.

[6] Wang B, Hu X, Lu P. Modelling and testing of large-scale masonry elements under three-point bending – Tough and strong nacre-like structure enlarged by a factor of 20,000. Eng. Fract. Mech. 2020;229:106961. https://doi.org/10.1016/j.engfracmech.2020.106961.

[7] Nguyen-Van V, Wickramasinghe S, Ghazlan A, Nguyen-Xuan H, Tran P. Uniaxial and biaxial bioinspired interlocking composite panels subjected to dynamic loadings. Thin-Walled Struct. 2020;157:107023. https://doi.org/10.1016/j.tws.2020.107023.

[8] Slesarenko V, Kazarinov N, Rudykh S. Distinct failure modes in bio-inspired 3D-printed staggered composites under non-aligned loadings. Smart Mater. Struct. 2017;26(3):035053. https://doi.org/10.1088/1361-665X/aa59eb.

[9] Ko K, Jin S, Lee SE, Lee I, Hong J-W. Bio-inspired bimaterial composites patterned using three-dimensional printing. Compos. Part B Eng. 2019;165:594–603. https://doi.org/10.1016/j.compositesb.2019.02.008.

[10] Tran P, Ngo TD, Ghazlan A, Hui D. Bimaterial 3D printing and numerical analysis of bio-inspired composite structures under in-plane and transverse loadings. Compos. Part B Eng. 2017;108:210–23. https://doi.org/10.1016/j.compositesb.2016.09.083.

[11] Rudykh S, Ortiz C, Boyce MC. Flexibility and protection by design: imbricated hybrid microstructures of bio-inspired armor. Soft Matter 2015;11(13):2547–54. https://doi.org/10.1039/C4SM02907K.

[12] Wegst UGK, Bai H, Saiz E, Tomsia AP, Ritchie RO. Bioinspired structural materials. Nat. Mater. 2015;14(1):23–36. https://doi.org/10.1038/nmat4089.

[13] Jia H, Li Y, Luan Y, Zheng Y, Yang J, Wang L, et al. Bioinspired Nacre-like GO-based bulk with easy scale-up process and outstanding mechanical properties. Compos. Part Appl. Sci. Manuf. 2020;132:105829. https://doi.org/10.1016/j.compositesa.2020.105829.

[14] Greco F, Leonetti L, Lonetti P. A novel approach based on ALE and delamination fracture mechanics for multilayered composite beams. Compos. Part B Eng. 2015;78:447–58. https://doi.org/10.1016/j.compositesb.2015.04.004.

[15] De Maio U, Fantuzzi N, Greco F, Leonetti L, Pranno A. Failure Analysis of Ultra High-Performance Fiber-Reinforced Concrete Structures Enhanced with Nanomaterials by Using a Diffuse Cohesive Interface Approach. Nanomaterials. 2020;10:1792. https://doi.org/10.3390/nano10091792.

[16] Greco F, Lonetti P. Mixed mode dynamic delamination in fiber reinforced composites. Compos. Part B Eng. 2009;40(5):379–92. https://doi.org/10.1016/j.compositesb.2009.03.003.

[17] Pascuzzo A, Yudhanto A, Alfano M, Lubineau G. On the effect of interfacial patterns on energy dissipation in plastically deforming adhesive bonded ductile sheets. Int. J. Solids Struct. 2020;198:31–40. https://doi.org/10.1016/j.ijsolstr.2020.04.001.

[18] Li J, Rudykh S. Tunable microstructure transformations and auxetic behavior in 3D-printed multiphase composites: The role of inclusion distribution. Compos. Part B Eng. 2019;172:352–62. https://doi.org/10.1016/j.compositesb.2019.05.012.

[19] Li J, Slesarenko V, Rudykh S. Auxetic multiphase soft composite material design through instabilities with application for acoustic metamaterials. Soft Matter 2018;14(30):6171–80. https://doi.org/10.1039/C8SM00874D.

[20] Greco F, Leonetti L, Lonetti P, Luciano R, Pranno A. A multiscale analysis of instability-induced failure mechanisms in fiber-reinforced composite structures via alternative modeling approaches. Compos. Struct. 2020;251:112529. https://doi.org/10.1016/j.compstruct.2020.112529.

[21] Bruno D, Greco F, Lonetti P, Blasi PN, Sgambitterra G. An investigation on microscopic and macroscopic stability phenomena of composite solids with periodic microstructure. Int. J. Solids Struct. 2010;47(20):2806–24. https://doi.org/10.1016/j.ijsolstr.2010.06.013.

[22] Nestorović MD, Triantafyllidis N. Onset of failure in finitely strained layered composites subjected to combined normal and shear loading. J. Mech. Phys. Solids. 2004;52(4):941–74. https://doi.org/10.1016/j.jmps.2003.06.001.
[23] Slesarenko V, Rudykh S. Microscopic and macroscopic instabilities in hyperelastic fiber composites. J. Mech. Phys. Solids. 2017;99:471–82. https://doi.org/10.1016/j.jmps.2016.11.002.
[24] Arora N, Batan A, Li J, Slesarenko V, Rudykh S. On the Influence of Inhomogeneous Interphase Layers on Instabilities in Hyperelastic Composites. Materials. 2019;12:763. https://doi.org/10.3390/ma12050763.
[25] Galich PI, Slesarenko V, Li J, Rudykh S. Elastic instabilities and shear waves in hyperelastic composites with various periodic fiber arrangements. Int. J. Eng. Sci. 2018;130:51–61. https://doi.org/10.1016/j.ijengsci.2018.05.003.
[26] Arora N, Li J, Slesarenko V, Rudykh S. Microscopic and long-wave instabilities in 3D fiber composites with non-Gaussian hyperelastic phases. Int. J. Eng. Sci. 2020;157:103408. https://doi.org/10.1016/j.ijengsci.2020.103408.
[27] Greco F. A study of stability and bifurcation in micro-cracked periodic elastic composites including self-contact. Int. J. Solids Struct. 2013;50(10):1646–63. https://doi.org/10.1016/j.ijsolstr.2013.01.036.
[28] Greco F, Leonetti L, Luciano R, Nevone Blasi P. Effects of microfracture and contact induced instabilities on the macroscopic response of finitely deformed elastic composites. Compos. Part B Eng. 2016;107:233–53. https://doi.org/10.1016/j.compositesb.2016.09.042.
[29] Greco F, Leonetti L, Medaglia CM, Penna R, Pranno A. Nonlinear compressive failure analysis of biaxially loaded fiber reinforced materials. Compos. Part B Eng. 2018;147:240–51. https://doi.org/10.1016/j.compositesb.2018.04.006.
[30] Greco F, Lonetti P, Luciano R, Nevone Blasi P, Pranno A. Nonlinear effects in fracture induced failure of compressively loaded fiber reinforced composites. Compos. Struct. 2018;189:688–99. https://doi.org/10.1016/j.compstruct.2018.01.014.
[31] Rudykh S, deBotton G. Instabilities of Hyperelastic Fiber Composites: Micromechanical Versus Numerical Analyses. J. Elast. 2012;106(2):123–47. https://doi.org/10.1007/s10659-011-9313-x.
[32] Miehe C, Schröder J, Becker M. Computational homogenization analysis in finite elasticity: material and structural instabilities on the micro- and macro-scales of periodic composites and their interaction. Comput. Methods Appl. Mech. Eng. 2002;191(44):4971–5005. https://doi.org/10.1016/S0045-7825(02)00391-2.
[33] Greco F, Luciano R. A theoretical and numerical stability analysis for composite micro-structures by using homogenization theory. Compos. Part B Eng. 2011;42(3):382–401. https://doi.org/10.1016/j.compositesb.2010.12.006.
[34] Silveirinha MG. Metamaterial homogenization approach with application to the characterization of microstructured composites with negative parameters. Phys. Rev. B. 2007;75:. https://doi.org/10.1103/PhysRevB.75.115104115104.
[35] Leonetti L, Greco F, Trovalusci P, Luciano R, Masiani R. A multiscale damage analysis of periodic composites using a couple-stress/Cauchy multidomain model: Application to masonry structures. Compos. Part B Eng. 2018;141:50–9. https://doi.org/10.1016/j.compositesb.2017.12.025.
[36] Greco F, Leonetti L, Lonetti P, Nevone Blasi P. Crack propagation analysis in composite materials by using moving mesh and multiscale techniques. Comput. Struct. 2015;153:201–16. https://doi.org/10.1016/j.compstruc.2015.03.002.
[37] Feo L, Greco F, Leonetti L, Luciano R. Mixed-mode fracture in lightweight aggregate concrete by using a moving mesh approach within a multiscale framework. Compos. Struct. 2015;123:88–97. https://doi.org/10.1016/j.compstruct.2014.12.037.
[38] Belytschko T, Loehnert S, Song J-H. Multiscale aggregating discontinuities: A method for circumventing loss of material stability: MULTISCALE AGGREGATING DISCONTINUITIES. Int. J. Numer. Methods Eng. 2008;73(6):869–94. https://doi.org/10.1002/nme.2156.
[39] Greco F, Leonetti L, Luciano R, Trovalusci P. Multiscale failure analysis of periodic masonry structures with traditional and fiber-reinforced mortar joints. Compos. Part B Eng. 2017;118:75–95. https://doi.org/10.1016/j.compositesb.2017.03.004.
[40] Greco F, Leonetti L, Pranno A, Rudykh S. Mechanical behavior of bio-inspired nacre-like composites: A hybrid multiscale modeling approach. Compos. Struct. 2020;233:111625. https://doi.org/10.1016/j.compstruct.2019.111625.
[41] Ji B, Gao H. Mechanical properties of nanostructure of biological materials. J. Mech. Phys. Solids. 2004;52(9):1963–90. https://doi.org/10.1016/j.jmps.2004.03.006.
[42] Khayer Dastjerdi A, Rabiei R, Barthelat F. The weak interfaces within tough natural composites: Experiments on three types of nacre. J. Mech. Behav. Biomed. Mater. 2013;19:50–60. https://doi.org/10.1016/j.jmbbm.2012.09.004.
[43] Meyers MA, Lin A-M, Chen P-Y, Muyco J. Mechanical strength of abalone nacre: Role of the soft organic layer. J. Mech. Behav. Biomed. Mater. 2008;1(1):76–85. https://doi.org/10.1016/j.jmbbm.2007.03.001.
[44] Barthelat F, Dastjerdi AK, Rabiei R. An improved failure criterion for biological and engineered staggered composites. J. R. Soc. Interface. 2013;10(79):20120849. https://doi.org/10.1098/rsif.2012.0849.
[45] Abid N, Mirkhalaf M, Barthelat F. Discrete-element modeling of nacre-like materials: Effects of random microstructures on strain localization and mechanical performance. J. Mech. Phys. Solids. 2018;112:385–402. https://doi.org/10.1016/j.jmps.2017.11.003.
[46] Radi K, Jauffres D, Deville S, Martin CL. Strength and toughness trade-off optimization of nacre-like ceramic composites. Compos. Part B Eng. 2020;183:107699. https://doi.org/10.1016/j.compositesb.2019.107699.
[47] Geymonat G, Muller S, Triantafyllidis N. Homogenization of nonlinearly elastic materials, microscopic bifurcation and macroscopic loss of rank-one convexity. Arch. Ration. Mech. Anal. 1993;122(3):231–90. https://doi.org/10.1007/BF00380256.
[48] Hill R. A self-consistent mechanics of composite materials. J. Mech. Phys. Solids. 1965;13(4):213–22. https://doi.org/10.1016/0022-5096(65)90010-4.
[49] Li J, Pallicity TD, Slesarenko V, Goshkoderia A, Rudykh S. Domain Formations and Pattern Transitions via Instabilities in Soft Heterogeneous Materials. Adv. Mater. 2019;31(14):1807309. https://doi.org/10.1002/adma.v31.1410.1002/adma.201807309.
[50] Li J, Slesarenko V, Galich PI, Rudykh S. Instabilities and pattern formations in 3D-printed deformable fiber composites. Compos. Part B Eng. 2018;148:114–22. https://doi.org/10.1016/j.compositesb.2018.04.049.
[51] Galich PI, Slesarenko V, Rudykh S. Shear wave propagation in finitely deformed 3D fiber-reinforced composites. Int. J. Solids Struct. 2017;110–111:294–304. https://doi.org/10.1016/j.ijsolstr.2016.12.007.